Suppressing Cracking in Resistance Welding AA5754 by Mechanical Means

Hongyan Zhang
Department of Mechanical, Industrial and Manufacturing Engineering,
University of Toledo,
Toledo, OH 43606

Jacek Senkara[1]
Department of Mechanical Engineering,
University of Michigan,
Ann Arbor, MI 48109

Xin Wu[2]
Department of Mechanical Engineering,
Wayne State University,
Detroit, MI 48202

In this paper mechanical aspects of cracking during single- and multi-spot welding of AA5754 was investigated by both experimental and analytical approaches. The impact of mechanical loading on crack initiation and propagation was studied with the consideration of various process parameters including the loading imposed by electrodes, the formation of liquid nugget, and constraining factors during and after welding. Tensile properties of AA5754 and their dependence on the temperature were tested at room and up to solidus temperatures, in order to provide a reference of cracking stress. Thermal-mechanical analysis was conducted based on the temperature field around the nugget and the state of stress encountered during welding. This analysis revealed that tensile stress might build up in the vicinity of the nugget during cooling, as explained in the experimental observation. General guidelines for suppressing cracking were proposed, i.e., to provide sufficient constraint around the weld spot during and after welding.
[DOI: 10.1115/1.1418693]

1 Introduction

Resistance spot welding (RSW) is a predominant means of body structure assembly in the automotive industry. Although this joining method has been used for many years, it is still more of an art than a science.

RSW of aluminum alloys has recently shown an increasing importance because of aluminum alloys' potential for weight reduction in automobiles [1–3]. It significantly differs from welding steel due to a number of substantial differences in mechanical, thermal, electrical, and metallurgical properties. One of the existing problems in fusion welding of some aluminum alloys is the susceptibility to cracking at temperatures close to solidus lines. The cracking phenomenon associates with existence of a wide solidus-liquidus gap, the presence of low melting point eutectics (e.g., Al-Cu, Al-Mg, and Al-Mg-Si) or impurities, high solidification shrinkage, large coefficient of thermal expansion, and a rapid drop of mechanical properties at elevated temperatures [4,5]. Although hot cracking theory in fusion welding and casting is nowadays well developed since the classic works of Pellini [6], Borland [7], and Prokhorov [8], cracking in RSW is not satisfactorily understood. Cracking in RSW aluminum alloy sheets was reported recently by Watanabe and Tachikawa [9], Michie and Renaud [10], and Thornton et al. [11]. However, the knowledge and understanding of cracking in fusion welding cannot be simply transferred to explain cracking in resistance spot welding. There is not sufficient information, nor a scientific explanation or theory on cracking in RSW Al alloys.

One mechanism of cracking in spot welding of AA5754 was proposed by Senkara and Zhang [12]. Based on this study, during RSW there exists favorable metallurgical conditions for cracking in the heat-affected zone (HAZ), i.e., the formation of liquid films surrounding solid grains, resulted from constitutional melting of the alloy and liquation of secondary phases (such as Al3Mg2) and impurities. These sub-zones of the HAZ with incomplete melting surround the liquid nugget. Such structures may be easily torn off when tensile stress or strain reaches a certain level.

In this study, cracking phenomena in single spot welds and the influence of constraining conditions and interactions between welds in multi-welded specimens are investigated. Through thermal-mechanical analysis of cracking mechanisms in both single and multi-spot welding, a cracking suppression methodology is proposed and verified by experiments.

2 Experimental Design

To understand the mechanical mechanisms of cracking in resistance spot welding of AA5754 and the influence of constraining conditions, a number of experiments were designed. These included creating cracking conditions using various sizes of specimens and types of electrodes, as well as welding under various constraining conditions.

Electrode Geometry: The effect of electrode geometry on cracking susceptibility was investigated using three kinds of electrodes. They are (see Fig. 1, based on the electrode classification of ''Resistance Welding Manual''[13]): **Type-A**: a crown-shaped tip with crown radius of 50 mm and tip diameter of 10 mm; **Type-B**: a dome-shaped tip with hemispherical radius of 8 mm; and **Type-C**: a truncated cone form with flat tip of 6 mm face diameter. Type-A is often used in resistance spot welding aluminum alloys, and Type-B and Type-C represent extreme cases of face geometry.

Specimens: The material used in this study was AA5754 alloy, the same as that used for the experiments in a previous work [12] for consistency. Sheets of 2.0 mm gauge in ''0'' temper condition (annealed) were surface pre-treated and pre-lubricated by the producer. The chemical composition specified by the producer is listed in Table 1, and some selected mechanical properties at room temperature are listed in Table 2. To understand how the specimen size influences cracking through constraining, coupons of three widths were used, i.e., 25 mm, 40 mm, and 90 mm. They are called narrow, medium, and wide (in width) hereafter for simplic-

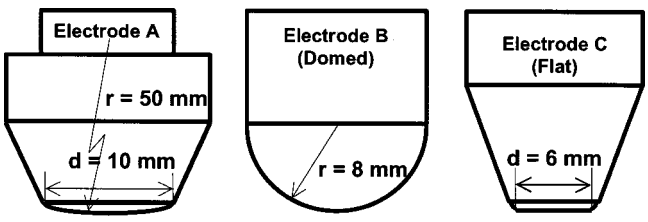

Fig. 1 Three types of electrodes (A, B, and C) used in tests

[1]On sabbatical leave from: Welding Department, Warsaw University of Technology, 85 Narbutta St., 02-524 Warsaw, Poland.

[2]Corresponding Author, Contact: Xin Wu, (313)577-3882, (Fax) 8789, xwu@eng.wayne.edu

Contributed by the Manufacturing Engineering Division for publication in the JOURNAL OF MANUFACTURING SCIENCE AND ENGINEERING. Manuscript received Sept. 2000; Revised May 2001. Associate Editor: Y. L. Yao.

Table 1 Chemical composition (Maximum value in wt. percent) of AA5754 (from [13])

	Mg	Mn	Cu	Fe	Si	Ti	Cr	Zn
Nominal	2.6-3.6	0.5	0.1	0.4	0.4	0.15	0.3	0.2

Table 2 Typical values of mechanical properties of AA5754 in "0" temper conditions (from [14])

Ultimate Tensile Stress	0.2 % Proof Stress	Elongation
225 MPa (32.6 ksi)	105 MPa (15.2 ksi)	26 %

ity. All the specimens were 160 mm long. The weld pitch in multi-spot welding was either 30 or 60 mm depending on constraining conditions.

Welding and Clamping Conditions: Welding was performed either with single- or multi-spot welding, with weld spot at the center of specimen width and along the longitudinal center (for multi-spot welding). Various specimen constraining conditions were simulated by clamping and by sequential welding (in multi-spot welding). Welding was conducted on a medium frequency (MF) DC welder, with primary AC frequency of 60 Hz. The welding parameter can be pre-set and it was repeatable. By recording the number of AC cycles the heating and cooling time can be accurately measured. During the entire welding time the electrode force was kept at 7 kN (measured through air pressure in an air cylinder supporting weld gun). The welding operation procedure was (in sequence): pre-heat at current of 3 kA for 50 ms (3 cycles), welding at current of 26 kA for 83 ms (5 cycles), and holding without current for 200 ms (12 cycles). The welding parameters were unchanged for all tests, so the effect of specimen/electrode geometry and welding sequence can be evaluated.

To verify the effect of constraining on cracking, steel washers were employed to clamp the workpieces at outside electrode region in single-spot welding, as shown in Fig. 2. Two sizes of steel washers were used: 65 mm/28 mm and 50 mm/22 mm (''outer diameter''/''inner diameter''). To study the shunting effect, for some tests a thin layer of insulator was also used in addition to the washers. It was cut into the shape of the washers, and placed between the workpieces. After welding all specimens were cut from the weld center along longitudinal or lateral directions. The cross-sections were ground, polished, and etched, followed by metallographic examination.

Mechanical Testing: In order to understand the cracking behavior of this aluminum alloy, tests of the ultimate tensile strength (UTS) and ductility at temperatures from RT up to the solidus temperature were conducted using an INSTRON tensile testing machine equipped with a furnace. The solidus and liquidus temperatures for this material are approximately 876 K and 915 K, respectively, determined by the chemical composition of the alloy (Table 1) and the equilibrium Al-Mg phase diagram [15].

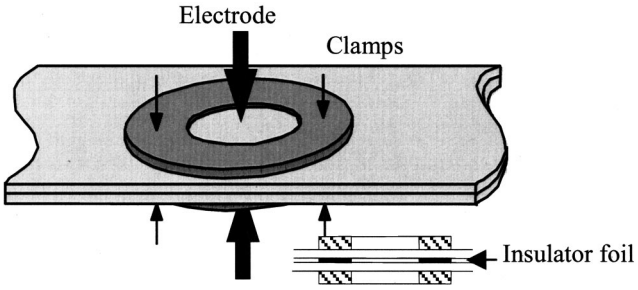

Fig. 2 Schematic for using constraining washers

3 Experimental Results

3.1 Cracking Observation. Optical microscopy inspection on the sectioned specimens indicates that this alloy has a high probability of cracking when resistance-welded, especially when Type-A electrodes were used. Metallurgical examination (see Fig. 3) shows that cracks mainly developed in the longitudinal (or specimen length) direction of the nugget and very few cracks appeared in the transverse (or width) direction of the specimens. Cracks initiated near the fusion line, and propagated into the HAZ along grain boundaries. In multi-spot welded specimens, cracks mainly appeared on the right side of the nuggets in consistence with the welding sequence (from left to right). In single-spot welding, from longitudinal section they were found mostly on both sides of the nugget.

It was found that the average directions for those cracks were at around 70 deg with respect to the fusion line tangential direction, as shown in Fig. 4. Upon propagation, the traces of many cracks were found to be slightly tilted away from their original directions, at a direction which coincides with the direction of the local temperature gradient (to be shown in the next section). This suggests that to some extent, thermal stresses induced by heating and cooling are responsible for crack initiation and propagation.

For multi-spot welded coupons that were sequentially welded

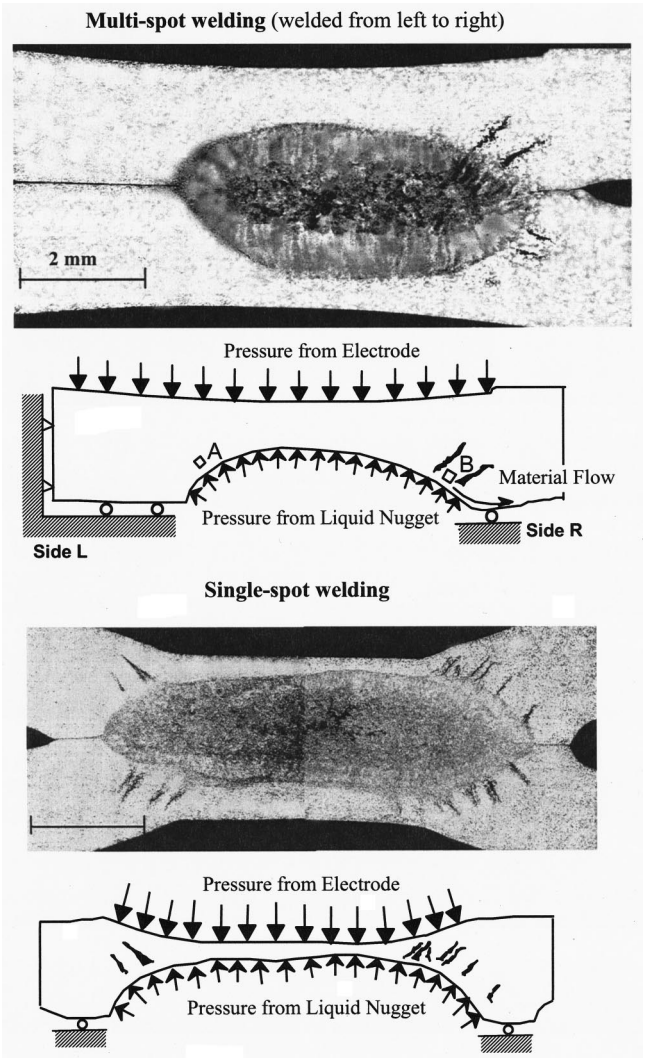

Fig. 3 Longitudinal cross-section of a multi-welded specimen (top) and a single welded specimen (bottom), with the representative loading and constraining conditions on half of the weldment. Locations "A" and "B" of multi-weld were used for stress analysis later.

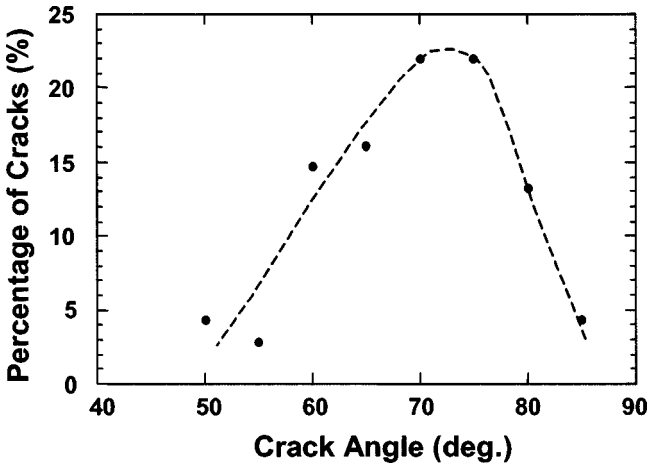

Fig. 4 Statistics of crack orientation angles (for nearly 70 cracks) with respect to the fusion line

along the central line of the specimens, interestingly, cracking always occurred on one side of the nugget that was towards unwelded specimen edge (i.e., away from the previous weld spots), while no cracking occurred on the welded side. In this case, they are clearly visible from longitudinal cross-sections in some distance from the fusion line, but invisible or visible as very narrow traces in transverse sections. If viewed from the longitudinal section, the cracked side (without previous weld) has a wider coupon separation gap than the side pre-welded, and some squeezed-out materials can be clearly seen inside the opened gap between coupons in the vicinity of nuggets.

Because metallurgical conditions in multi-spot welds are identical to that in the previous single-spot weld, the only difference is that in multi-spot welding its one-side edge was constrained by the previous welds. This finding strongly suggests that the mechanical constraints play a critical role in cracking. Thus, we need to investigate the mechanical cause for cracking.

A series of experiments were carefully designed and conducted under various constraining conditions, including combinations of various specimen sizes, electrode geometry and welding sequence. Two additional electrode geometries with drastically different faces were used in this part of the study. They were Type-B electrode (with a domed face, called ''domed'' electrode hereafter) and Type-C electrode (with a flat face, called ''flat'' electrode hereafter, as given in Fig. 1). With different contacting conditions, these two types of electrodes represent two extreme cases. The cracking results are examined and represented using the average number and total length of cracks on each weld, obtained over at least three specimens (replicates). All testing conditions and cracking results are summarized in Figs. 5–9, and Table 3. The detailed explanation on these results is also given below.

3.2 Effect of Specimen Width and Electrode Geometry on Cracking. Three coupon widths, (25 mm, 40 mm, and 90 mm,) with both flat and domed electrodes were used, and the resulting cracking tendencies are given in Fig. 5. The increase in coupon width can significantly reduce cracking tendency for both domed and flat electrodes. Because specimen width provides a natural constraining on the bending or separation of sheets, there would be less sheet distortion in wider specimens. In addition, wider specimens provide larger mass and reduce peak temperature or thermal stress. Therefore, the influence of specimen width on cracking can be well understood.

As for the effect of electrode geometry, specimens welded using domed electrodes show a significantly larger number of cracks and crack lengths than the ones using flat electrodes, for all coupon widths. Metallographic examination indicates that with small radius domed electrodes significant material flow occurred, and

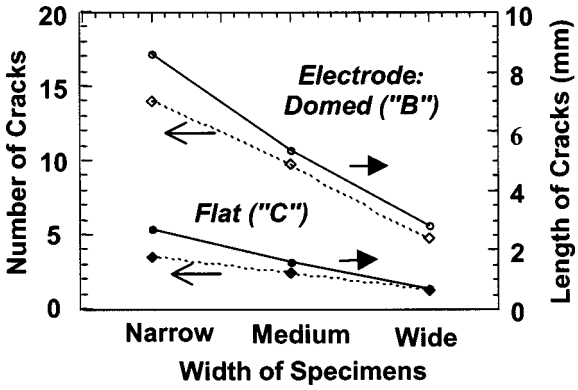

Fig. 5 Influence of specimen size and electrode type on cracking in single-spot welding

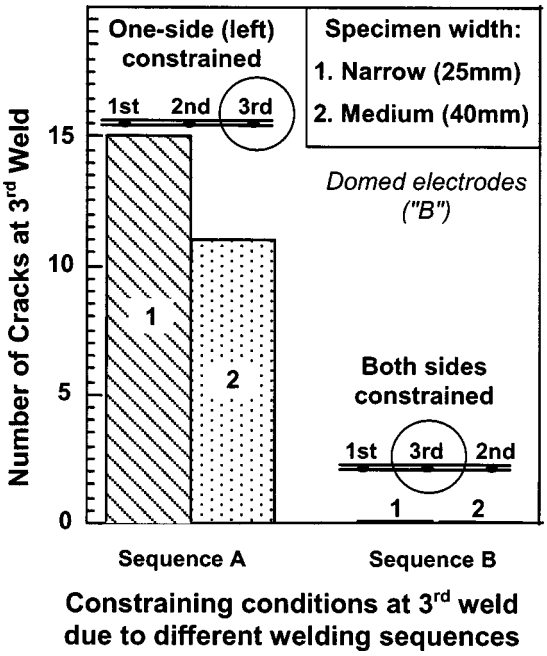

Fig. 6 Effect of welding sequence. Sequence A on the left: the 3rd welding was constrained on one-side only, and cracking occurred on the unconstrained (open) side; Sequence B on the right: the 3rd welding was constrained on both sides, and no cracking was observed.

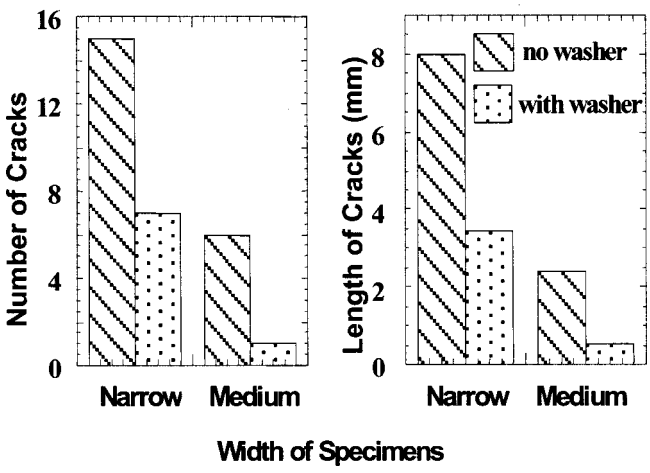

Fig. 7 The effect of constraining washers on cracking tendency. Domed electrodes were used.

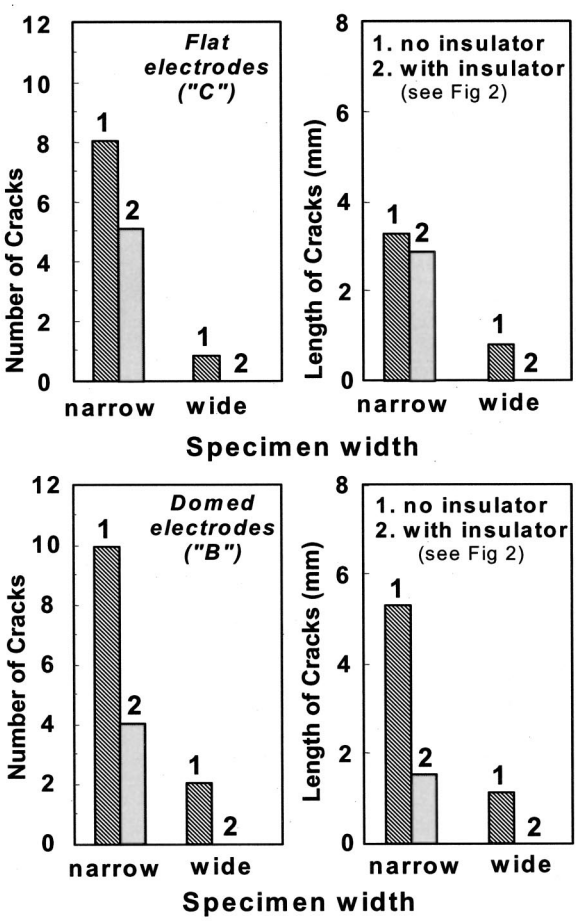

Fig. 8 Influence of insulating between workpieces on cracking. Welding with domed electrodes (top) and flat electrodes (bottom), respectively.

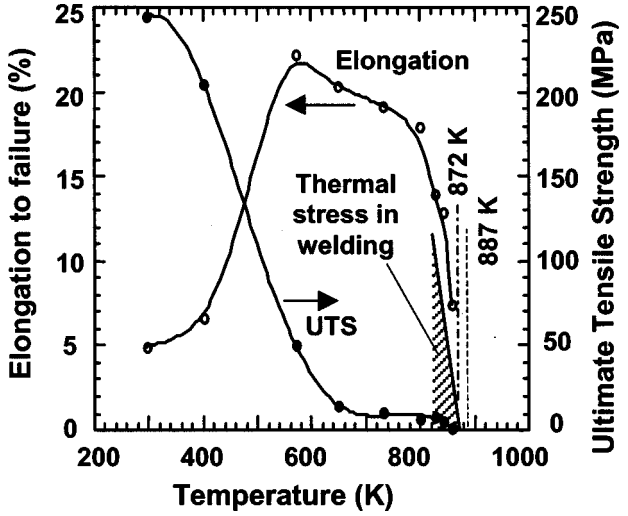

Fig. 9 Dependence of ductility and ultimate strength (UTS) on temperature. Dashed lines mark the solidus temperatures (887 K and 872 K) for AA5754 with Mg content ranging from 2.6–3.6 wt. percent. The shadowed area indicates possible thermal stress range in the HAZ.

Table 3 Dependence of cracking tendency on welding conditions/variables

Variable	Influence on Cracking
Electrode type	Domed (+); Flat (–)
Increase in specimen width	(–)
Constraining by washer	(–)
Constraining by neighboring welds	(–)
Using insulator with washers	(0)

Note: (+) — increasing cracking tendency
(–) — decreasing cracking tendency
(0) — no clear influence on cracking

large separation was produced at the edge of the nugget. Compared with flat electrodes, domed electrodes provide smaller contact area between the electrode/workpiece and between workpiece/workpiece interfaces. This can yield two effects: (1) the localized electrode contact produces a higher and non-uniform contact stress on the interface, with less constraining to the specimen distortion, (2) domed electrodes provide higher current density and heating rate (or temperature gradient). As a result, larger distortion and cracking tendency are expected. In addition, such a domed electrode tends to cause expulsion, which also contributes to cracking [12].

3.3 Effect of Welding Sequence on Cracking. In multi-spot welding two welding sequences, *Sequence A (1,2,3)* and *Sequence B (1,3,2)* were compared, where the numbers are the labels of the sequential welding spots along the longitudinal strip. The difference between these two sequences is that in Sequence B the third weld was made under the condition that both ends of the specimen were constrained by the two previous welds (weld-1 & -2) while for Sequence A only one side (left) was constrained. The cracking tendency, indicated by the total number of cracks on three specimens in each case, for the two welding sequences with various coupon widths, is shown in Fig. 6. The total number of cracks reduced to zero when welds were made with constraining from neighboring welds (Sequence B), compared with the case of having constraining welds only on one side (Sequence A). It was also found that in the both-end constrained case the cross-sectional area of the nugget was slightly smaller. Apparently the constraint in Sequence B reduced the workpiece distortion, and possibly provided additional electric current shunting path and reduced current density.

3.4 Effect of Washer Clamping on Crack Suppression. To further verify the cracking mechanisms and provide a means of crack suppression, additional constraint was applied prior to welding to the electrode surrounding through two steel washers. Two pieces of aluminum sheets were put together with one washer on each side. The whole stack-up was held by two C-clamps, as previously illustrated in Fig. 2. The electrodes were then put through the openings of the two identical washers on both sides of the sheets, and a weld was made between the sheets inside the clamped area. The comparison of cracking tendency between specimens welded with and without washers, as well as between medium and narrow coupons is shown in Fig. 7. When washers were used, the number of cracks and the total crack length (on three specimens in each case) are significantly reduced for both medium and narrow coupons, but the reduction is more significant in medium size coupons. The metallographic examination shows that with washer application the distortion is significantly reduced, and the sheet separation is localized, within a ring-shaped opening area surrounding the nugget, and it diminishes at the places where sheets were clamped by the washers. Virtually no material flow at the faying interface near the nugget was observed. No significant difference was found between results from different washer sizes.

3.5 Effect of Current Shunting on Cracking. To understand the influence of current shunting on cracking tendency from washer application, a comparison was made between welding with and without a thin layer of insulator inserted between the two sheets to be welded. As shown in Fig. 8 where cracking tendency is expressed by the total number and length of cracks on three specimens in each case, depending on the shape of electrodes used, the effect of insulator on cracking is slightly different, but in general, this effect is insignificant. For the domed electrode cases, using insulators reduces cracking tendency for all specimen widths tested, and the same trend was seen for flat electrode with wide specimens, but no effect was detected for flat electrodes with narrow specimens. It appears that the shunting effect does exist for most cases except for flat electrode-narrow specimen cases. The local deformation also shows the difference with and without insulators. When domed electrodes were used, welds with insulators show significantly less distortion at the periphery of the nugget than the ones without insulators. However, metallographic examination shows that there is no significant difference in nugget size and penetration with and without insulators. The insulator inserted between the specimen sheets changes the contact resistance and affects heat generation, yet the exact effect of insulators is not very clear at this time.

The major findings described above on the effects of the welding variables on the cracking are summarized in Table 3. The interactions of these variables are not listed in the table. The basic principles or mechanisms discussed in this paper should be applicable in various practical problems.

3.6 Material Strength and Ductility at Various Temperatures. Cracking is a competing process between applied stress and material cracking resistance, the latter is related to the material strength and ductility, thus uniaxial tensile test was conducted at various temperatures. The tested results of ductility, represented by the total elongation to failure, are shown in Fig. 9. Elongation increases with temperature, and it reaches its maximum at about 580 K. Further increase in temperature causes the decrease of ductility, with a dramatic drop of elongation at above 800 K. The ultimate strength (UTS) monotonically decreases with increasing temperature, and it becomes as low as 10 MPa for temperatures above 700 K. The measured UTS at near solidus temperature ($\sim$876 K) is close to zero (or beyond the measurable range of the current setup). It can be seen from the figures that both strength and ductility of the alloy at sub-solidus temperatures are extremely low. As for the thermal stress during welding, an estimation of the possible stress range (shown in the shaded area of Fig. 9) will be given in the next section.

4 Thermal-Mechanical Analysis of Cracking Mechanisms

The distinct cracking characteristics between the single- and multi-spot welding strongly suggests that, besides the metallurgical effect (that provides a driving force of cracking due to volume change involved in melting-solidification cycle), thermal-mechanical factors play an important role in the initiation and subsequent propagation/growth of cracks. Therefore, this section is devoted to the mechanisms of crack formation by thermal-mechanical analyses using simplifying assumptions. Qualitative, rather than quantitative analysis, was performed because there is no feasible accurate analysis for such a complicated cracking process.

4.1 Thermal Stress Development. In resistance welding, due to the direct heating by Joule heat and rapid cooling by water-cooled electrode and by heat conduction from the large mass of workpieces, high temperature gradients and thermal stress develop during heating and cooling in the HAZ, which participate the force equilibrium with the mechanical loading.

The influence of thermal stressing on crack initiation and propagation can be estimated based on the thermal history. A thermal-mechanical analysis can start with multi-spot welded nuggets because of the characteristic appearance of cracking only on one side of the nuggets. As mentioned earlier, cracks appear on the same sides of the nuggets, in accordance with the welding sequence in a multi-spot welded strip, while no significant crack trace has been found on other sides of the nuggets. In contrast, cracks are often seen on both sides of a single weld, as shown in Fig. 3.

It can be seen that there is a solid material flow on the cracking side (Side R) as the material in the HAZ is squeezed out during heating, which forms a blunt notch-shaped edge and generates a large sheet separation. To the contrary, no solid deformation and separation can be observed on Side L. This uneven deformation or asymmetric geometry is the consequence of uneven thermal-mechanical loading on the two sides during welding.

The mechanical loading conditions that caused cracking (shown in Fig. 3) are schematically represented underneath each micrograph in Fig. 3, for multiple spot welding (top) and single spot welding (bottom), respectively. On Fig. 3-top, the loading on one sheet can be simplified as the pressure from the electrode, the pressure from the liquid nugget [16], the response force from the other sheet, plus the constraining force from the previous weld that is on the left side only. For the right side, and for single weld shown in Fig. 3 (bottom), the loading conditions are similar except that there are no constraining forces to prohibit sheets separation. By volume expansion during heating material plastic flow occurred on the unconstrained side, and blunt notch-shaped edges formed, see Fig. 3 top-right side and bottom both sides. Consequently, cracking occurred in all such cases.

To better understand the mechanism of cracking, we take material at two characteristic locations A and B from the two sides near the fusion line for examination (see Fig. 3 top). The thermal stresses development in the solid (HAZ) during heating and cooling are outlined below.

(1) Thermal stress during heating: The solid phase between the electrodes and the liquid nugget tend to expand during heating. At location A, a large compressive stress is developed in the direction parallel to the isotherms during heating or expansion, due to constraints from the solid phase of the sheets on Side L. At location B on Side R, however, there is very little compressive stress build-up in the vicinity of the nugget, because the solid phase can expand more freely and the sheets are free to separate, which effectively releases the stress at B. The stresses at A and B are schematically shown in Fig. 10-heating.

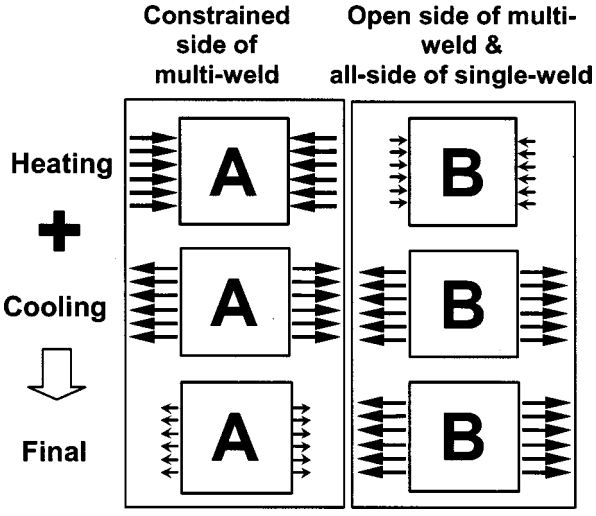

Fig. 10 Possible stresses during heating, cooling, and combined final stress states at locations A and B taken from Fig. 3

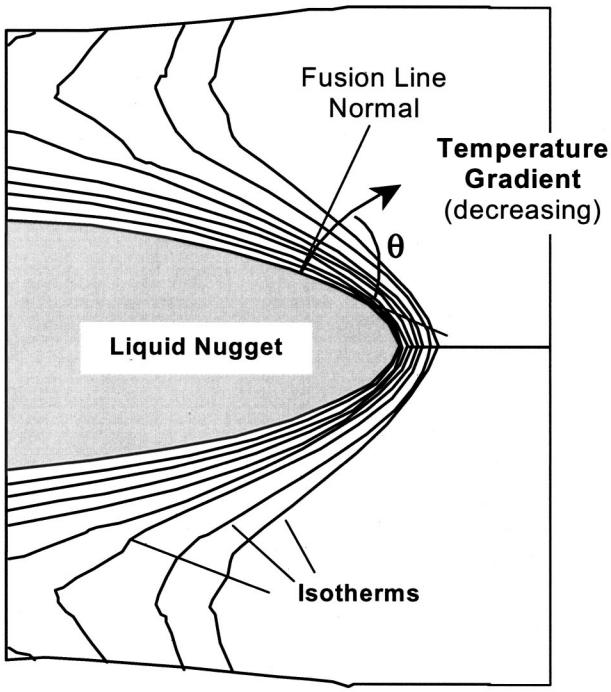

Fig. 11 Temperature distribution by a finite element analysis at the moment when heating is stopped. The temperature is the highest in the liquid nugget that is beyond the melting point.

(2) Thermal stress during cooling: When the electrical current is shut off, heating is terminated and rapid cooling starts. In fact, cooling is provided by the electrodes and workpiece during the entire period of welding, but its rate is much higher after the electric current is shut off. Tensile stresses develop at locations A and B at equivalent magnitude during shrinking under the constraining from their outside surrounding (Fig. 10-cooling). For location B, the solid material displaced during heating can hardly be sucked back due to lower temperature (or higher yield strength) and the constraint from the solid phase in the HAZ, especially in the region previously squeezed out.

(3) Final states of stress: The stress states of locations A and B during heating and cooling are superimposed. The final states of stress can be simplified as Fig. 10-final. It can be seen that the resultant stress at B is in tension, and that at A is very small (either tensile or compressive). The tensile stress at B during cooling is directly responsible for crack initiation in the region. In the case of a single weld, the stress state on both sides of the nugget is similar to the one at location B of the multi-spot weld, which has a final stress in tension.

4.2 Crack Orientation. Using a finite element model [17], a temperature distribution at the end of heating was generated as shown in Fig. 11. Because of cooling through the electrodes and workpieces, isotherms in the HAZ appear dense around the nugget, which is similar to the results of many others, such as that by Gupta and De [18]. The cooling temperature gradient turns towards the radial direction from the fusion line.

The tensile stress developed during cooling is approximately along the tangent of the isotherm near the nugget. Therefore, the orientation of a crack, which is normal to the direction of maximum tension, is approximately normal to the tangent, i.e., along the temperature gradient. The slight deviation of the measured result (70 deg rather than 90 deg) from the normal direction is probably due to other effects such as liquid pressure and applied vertical load from electrodes. For the same reason, at the places away from the fusion line, the change of the crack orientations during propagation can be explained due to the change of temperature gradient, as shown in Fig. 11.

4.3 Estimation of Thermal Stress. A simple calculation of thermal stress provides an estimate of the stress level at location B. Right after electrical current is shut off, strain in the direction parallel to the fusion line can be estimated by considering elastic and thermal strain components:

$$\varepsilon = \frac{\sigma}{E} + \alpha \Delta T \tag{1}$$

where ε is the total strain, σ, the stress, E, Young's modulus, α, coefficient of thermal expansion, and ΔT, the temperature drop during cooling. The tensile stress at B should be between two extreme cases, (a) lower bound: $\sigma=0$ (when $\varepsilon=\alpha\Delta T$, unconstrained, or free to shrink) (b) upper bound: $\sigma=E\alpha(-\Delta T)$ (when $\varepsilon=0$, fully constrained). The true value of stress at B depends on the actual constraining.

If we take $E=70$ GPa and $\alpha=33\times10^{-6}\,\mathrm{K}^{-1}$ [19] and use Eq. (1) the stress range is plotted in Fig. 9 by the shaded area. For a temperature drop $\Delta T=-50$ K, the stress range at B at temperature just below the solidus temperature is 0~115 MPa (in tension). In this range, the thermal stress developed near the solidus during cooling in the solid phase is possible to be high enough to initiate cracks, considering the strength (UTS) shown in Fig. 9. The rapid drop of ductility near the melting point may also contribute to crack initiation.

4.4 Discussion On Other Mechanical Factors. Along with stresses developed due to thermal expansion and shrinkage, mechanical loading and constraining caused by other processes also contribute to crack initiation and propagation. The most influential one is probably the effect of liquid pressure generated during melting and volume expansion in the nugget onto its surrounding solid. As shown in Fig. 10, liquid metal imposes a high pressure onto the solid in the direction normal to the fusion line. The resultant force from the liquid pressure is also partially responsible for workpiece separation (if no mechanical constraint). Indeed it was observed that when expulsion happened, the ejection of liquid metal pushed or bent the solid at a high speed. Obviously, this induces strain at a high strain rate in the solid surrounding the liquid nugget, and the region under the greatest straining is that near the edge of the nugget, either in the state between solidus and liquidus, or where liquid films exist at grain boundaries, with brittle structures of low strength [12]. And according to the theory proposed by Prokhorov [20], hot cracking may occur when the structure is in the brittle temperature range.

From the above observation and analysis it can be seen that constraining, either from pre-welded end or from the surrounding solid and the electrode, is beneficial for suppressing cracking in spot welding aluminum alloys. This conclusion is quite different from the general observations in fusion welding (e.g., arc welding), where cracking susceptibility increases with the degree of restraint. This can be understood if we realize that, in resistance spot welding the heat is generated inside the workpiece (at the interface of two sheets), and the liquid nugget is surrounded by solid. Accordingly, the constraining can provide a high pressure within the melt and a compressive stress in its surrounding during heating, and reduces the tensile stress in cooling. While in the case of arc welding the liquid pool is opened, so that any constraints from the surrounding solid will prohibit material flow into the weldment during cooling/shrinking, thus increasing the tendency of cracking, and a net tensile stress will be generated.

5 Summary

The cracking phenomenon in single and multiple resistance spot welding of AA5754 was investigated experimentally, and

analyzed using simplified thermal-mechanical models. The major findings related to the mechanisms of cracking can be summarized as follows:

- Tensile thermal stress is developed on the nonconstrained side of the weldment in the cooling stage of welding in multi-spot welds and on both sides of single spot welds.
- The value of this thermal stress at the temperature just below the solidus temperature is estimated to be comparable with, or higher than the measured strength of the material at elevated temperatures. Therefore, a high probability of crack formation and propagation exists in the region adjacent to the nugget, where solid and liquid phases co-exist.
- Unlike fusion welding processes, constraining in resistance spot welding is preferred for minimizing cracking, because it reduces the tendency of generating tensile stresses in the HAZ during welding.
- Cracking tendency is affected by various welding parameters and constraining conditions, such as welding electrode geometry, specimen geometry (width), post-welding reversed bending, welding sequence, and expulsion.

Based on the understanding of crack formation mechanisms and affecting factors during resistance sport welding of AA5754 alloys, the general trends and approaches to suppressing cracking are proposed:

- In product and assembly design the minimum width of the parts to be welded by resistance spot welding should be wide enough to avoid bending induced cracking during welding. Other constraining mechanisms, such as flanged specimens, may also serve this purpose.
- The electrode geometry should be carefully chosen, since it affects the formation of welding cracks. In most cases flat electrodes hinder cracking, though other factors need to be considered.
- In assembly process design the welding sequence needs to be considered in order to minimize cracking. In general, welding two ends first will provide a better constraint to the middle welding, thus reducing the chance of cracking.
- In fixture design it would be helpful to locate the clamping near the welding area. Additional clamping around the weld tip can provide better constraining from sheet bending and distortion, thus greatly reducing the chance of cracking.
- A combination of the aforementioned approaches, including the use of supporting washers around the electrodes for additional constraining, can provide an effective means of suppressing cracking.

Acknowledgment

The authors would like to thank Mr. Douglas R. Boomer, Alcan Aluminum Company, and Mr. David A. Androvich, Robotron Corporation, for their assistance in experiments.

References

[1] Warren, A. S., 1991, ''The Future for Increased Use of Aluminum in Cars,'' Aluminum, **67**(11), pp. 1078–1080.
[2] Osterman, F., 1993, *Aluminum Materials Technology for Automobile Construction*, Mechanical Engineering Publications Ltd, London.
[3] Irving, B., 1995, ''Building Tomorrow's Automobiles,'' Weld. J. (Miami), **74**(8), pp. 29–34.
[4] *Welding Handbook Volume 3: Materials and Applications—Part 1*, 1996, 8th Edition, AWS, Miami, FL, pp. 18–19.
[5] Anik, S., and Dorn, L., 1991, ''Metal Physical Processes During Welding—Weldability of Aluminum Alloys,'' Welding Research Abroad, **XXXVII**, pp. 41–44.
[6] Pellini, W. S., 1952, ''Strain Theory of Hot Tearing,'' Foundry Trade J. **80**, pp. 125–133.
[7] Borland, J. C., 1961, ''Suggested Explanation of Hot Cracking in Mild and Low Alloy Steel Welds,'' British Welding Journal, **8**, pp. 526–540.
[8] Prokhorov, N. N., 1968, ''Theorie und Verfahren zum Bestimmen der Technologischen Festigkeit von Metallen beim Schweissen,'' Schweisstechnik, **19**, pp. 8–11.
[9] Watanabe, G., and Tachikawa, H., 1995, ''Behaviour of Cracking Formed in Aluminum Alloy Sheets on Spot Welding,'' 48th Annual Assembly of IIW, Stockholm, IIW Doc. No III-1041-95.
[10] Michie, K. J., and Renaud, S. T., 1996, ''Aluminum Resistance Spot Welding: How Weld Defects Affect Joint Integrity,'' *Proc. AWS Sheet Metal Welding Conference VII*, Detroit, MI, Paper No. B5.
[11] Thornton, P. H., Krause, A. R., and Davies, R. G., 1996, ''The Aluminum Spot Weld,'' Weld. J. (Miami), **75**(3), pp. 101-s to 108-s.
[12] Senkara, J., and Zhang, H., 2000, ''Cracking in Multi-Spot Welding Aluminum Alloy AA5754,'' Weld. J. (Miami), **79**(7), pp. 194-s to 201-s.
[13] *Resistance Welding Manual*, 1946, the Resistance Welder Manufacturers' Association.
[14] *Automotive Sheet Specification*, 1994, Alcan Rolled Products Company, Feb.
[15] *Binary Alloy Phase Diagrams*, 1990, Massalski, T. B., ed., 2nd Ed., ASM, Materials Park, OH.
[16] Senkara, J., Zhang, H., and Hu, S. J., 2001, ''Expulsion Prediction in Resistance Spot Welding,'' Weld. J. (Miami), in press.
[17] *Aluminum: Properties and Physical Metallurgy*, 1984, Hatch, J. E., ed., ASM, Metals Park, OH.
[18] Zhang, H., Huang, Y., and Hu, S. J. 1996, ''Nugget Growth in Spot Welding of Steel and Aluminum,'' *Proc. AWS Sheet Metal Welding Conference VII*, Detroit, MI, Paper No. B3.
[19] Gupta, O. P., and De, A., 1998, ''An Improved Numerical Modeling for Resistance Spot Welding Process and Its Experimental Verification,'' ASME J. Manuf. Sci. Eng., **120**, pp. 246–251.
[20] Prokhorov, N. N., 1968, ''Theorie und Verfahren zum Bestimmen der Technologischen Festigkeit von Metallen beim Schweissen,'' Schweisstechnik, **19**, pp. 8–11.